Structural comparison of metarhodopsin II, metarhodopsin III, and opsin based on kinetic analysis of Fourier transform infrared difference spectra

Alexandra L. Klinger and Mark S. Braiman
Department of Biochemistry, University of Virginia Health Sciences Center, Charlottesville, Virginia 22908 USA

ABSTRACT Fourier transform infrared difference spectra were measured at 30-s intervals after a complete bleach of rhodopsin (rho) samples at 20°C and three different pH values. At each pH, all of the spectra could be fit globally to two exponential decay processes. Using a branched unimolecular kinetic model in which metarhodopsin II (meta II) is hydrolyzed to opsin and retinal both directly and through metarhodopsin III (meta III), we calculated rho → meta II, rho → meta III, and rho → opsin difference spectra at each of the pH values and obtained estimates for the microscopic rate constants at each pH. Because of assumptions that had to be made about the branching ratio between the meta II decay pathways, some uncertainties remain in our calculated rho → meta III difference spectrum at each pH. Nevertheless, our data covering long time ranges, especially those obtained at pH 8, place significant new constraints on the spectrum of meta III and thus on its structure. The rho → meta II spectrum shows no significant pH dependence over the range examined (pH 5.5–8). However, the rho → meta III and rho → opsin spectra each include a limited subset of pH-dependent peaks, which are mostly attributable to titratable amino acid side chains. Our observations can be used to refine an earlier conclusion that the visual pigment refolds to a rhodopsin-like conformation during meta II decay (Rothschild, K. J., J. Gillespie, and W. J. DeGrip. 1987. *Biophys. J.* 51:345–350). Most of this refolding occurs in the same way at pH values ranging from 5.5 to 8 and whether meta II decays to meta III or opsin. Meta II displays unique spectral perturbations that are mostly attributable to a few residues, probably including three to four aspartic or glutamic acids and an arginine.

INTRODUCTION

Rhodopsin (rho)[1], the main protein component of the outer segment of rod cells in the vertebrate retina, is comprised of a molecule of 11-*cis* retinal bound to Lys-296 of the apoprotein (opsin) through a protonated Schiff base linkage. When the retinal absorbs a visible photon, it isomerizes to the all-*trans* configuration. This event triggers a series of structural changes in the protein. Since these changes affect the absorption maximum of the chromophore, the kinetics of formation of the various photointermediates have been well characterized by visible spectroscopy (1).

Metarhodopsin II (meta II) has been identified as "Rho*," the "active" species that interacts with the G-protein transducin, catalyzing its binding of guanosine triphosphate in exchange for guanosine diphosphate (2, 3). This activation process initiates a cascade of reactions that ultimately results in the electrical hyperpolarization of the rod cell membrane (4). A metastable equilibrium between meta II and its "inactive" precursor, metarhodopsin I (meta I), is formed within milliseconds after light is absorbed (5). At physiological temperatures, meta II begins to decay into another inactive form, metarhodopsin III (meta III), within a few seconds (6). Meta III subsequently decays into a mixture of retinal and opsin via hydrolysis of the Schiff base linkage (7).

Relatively little is understood about which protein structural changes involved in the formation of meta II are important for its recognition by transducin. Comparisons of infrared (IR) spectra of meta II, and its inactive decay products, meta III and opsin, are likely to aid in this understanding. The decay of meta II at 20°C was previously studied with Fourier-transform IR (FTIR) difference spectroscopy (8). However, the data covered limited temporal and spectral ranges, and no attempt was made to deconvolute the individual spectral contributions of meta II, meta III, and opsin. In other work, FTIR difference spectra of individual rhodopsin photointermediates have been obtained by trapping these intermediates at low temperature (9). However, it has not been possible to trap meta III in this manner, because any temperature high enough to permit the meta II → meta III conversion also permits meta III → opsin decay. As a result, the rho → meta III IR difference spectrum has not been obtained previously.

In this work, we have succeeded in deriving this difference spectrum by performing a detailed kinetic analysis on rhodopsin photoproduct FTIR spectra extending to long times after photobleaching. Singular value decomposition (SVD) was used to reduce the complexity of the data, allowing a global fit to sums of exponentials. Using the rate constants derived from this fitting procedure, in combination with a commonly accepted model for the allowed decay pathways, not only the rho → meta III difference spectrum but also rho → meta II and rho → opsin + retinal spectra were calculated.

These spectra were all obtained at the same temperature (20°C) where it has been shown directly that the

Address correspondence to Mark Braiman.

[1] *Abbreviations used in this paper:* FTIR, Fourier-transform infrared; IR, infrared; meta I, metarhodopsin I; meta II, metarhodopsin II; meta III, metarhodopsin III; rho, rhodopsin; ROS, rod outer segments; SVD, singular value decomposition.

0006-3495/92/11/1244/12 $2.00

decay in the ability of rhodopsin to activate G-protein is concurrent with the decay of meta II to either meta III or opsin (3). Thus, no temperature effects can be responsible for differences between the spectra we derived for the three photoproducts. Therefore, we can confidently distinguish in our spectra structural features that are unique to meta II and thus likely to be involved in G-protein binding and activation.

MATERIALS AND METHODS

Preparation of disk membranes

Rod outer segments (ROS) were isolated from frozen bovine retinas by a sucrose flotation method described elsewhere (10). The ROS were washed isotonically to remove soluble proteins and then hypotonically to remove extrinsic membrane proteins. The resulting washed disc membranes were incubated for 8 h in Ficoll and subsequently floated in a centrifuge (85,000 g, 4 h) to remove any nonintact discs. Before being put in the FTIR spectrometer, the membranes were washed twice in the measurement buffer (30 mM NaCl, 6 mM KCl, 2 mM $MgCl_2$, 10 mM tris(hydroxymethyl)-aminomethane or 2-(*N*-morpholino)ethanesulfonic acid buffer), and centrifuged (80,000 g, 1.5 h) to form a tightly packed pellet. A portion of this pellet was blotted on a hydrophilic membrane (GVWP filter disk; Millipore Corp., Bedford, MA) to remove additional water and then transferred to a 19-mm-diam Ge window (used to protect the sample from photolysis by stray reflections from the spectrometer's HeNe laser reference beam). A second window (of CaF_2), the edges of which were coated with a thin layer of vacuum grease to prevent loss of water, was used to squeeze the sample to a thickness of $\sim$10 μm. The water content of the samples ranged between 50 and 60% water by weight as determined by the IR spectra (11).

FTIR measurements

All FTIR measurements were made using a Nicolet 60 SXR spectrometer (Madison, WI) with a Hg-Cd-Te detector. The interferometer retardation velocity was 5.8 cm s^{-1}; each interferogram consisted of 4,608 data points, giving 4 cm^{-1} resolution. The sample holder was a temperature-controlled flow-through cell (Harrick Scientific, Ossining, NY) connected to a water bath thermostatted at 293 K.

Spectra were measured every 30 s; each consisted of an average of 512 scans. Each sample was kept in the dark while the sample compartment was purged with dry air, until a stable spectral baseline was obtained ($\sim$4 h). The sample was then illuminated for 60 s using a filtered slide projector lamp ($\lambda > 500$ nm). This light was directed into the sealed sample compartment and onto the transparent (CaF_2) side of the sample holder by means of a fiber optic illuminator (Dolan-Jenner Industries Inc., Woburn, MA). Spectra continued to be measured every 30 s during illumination and for an additional $\sim$2 h afterward. The time series of absorbance difference spectra was obtained by ratioing each of the postillumination spectra to the last preillumination spectrum and then taking the negative logarithm.

Kinetic analysis

SVD was performed using a computer routine from the International Math and Statistics Library (IMSL, Houston, TX) as described previously (12). The time courses resulting from the SVD were fit to sums of exponentials using a nonlinear fitting program (13). Further calculations and plotting of spectra were performed using PC-Matlab (The MathWorks, South Natick, MA) and Lab-Calc (Galactic Industries, Salem, NH).

RESULTS

Temporal evolution of the difference spectrum

A typical time series of rho photointermediate difference spectra, covering $\sim$2 h, is illustrated in the top part of Fig. 1. The absorbance change relative to the unbleached sample is plotted on the *z*-axis as a function of both spectral frequency (*x*-axis) and time after illumination (*y*-axis).

The earliest difference spectrum (at the front of the mesh plot) is essentially identical to published rho $\rightarrow$ meta II difference spectra (9, 14). In subsequent spectra, there is a sharp decrease in the magnitude of both positive and negative bands in the amide I ($\sim$1,650 cm^{-1}) and amide II ($\sim$1,550 cm^{-1}) regions. Such decreases indicate that the protein returns to a more rho-like structure during the meta II decay, as shown previously by FTIR (8). This earlier study examined solely this fast initial refolding process. In contrast, our data extend to longer times after bleaching. We were thus able to detect a slower subsequent process, which actually involved a change in the sign and a subsequent increase in magnitude of several difference bands (e.g., $\sim$1,555-cm^{-1} band in Fig. 1), inconsistent with a simple refolding phenomenon.

The time series obtained from the lower pH experiments (data not shown) are qualitatively similar to those in Fig. 1. Again, the earliest difference spectra are clearly due to the rho $\rightarrow$ meta II transition, and the presence of at least two distinct decay processes for meta II is evident.

Singular value decomposition

To deconvolute the individual contributions of the spectral intermediates involved in the meta II decay process, it was necessary to fit the spectral data in the region of interest (1,800–1,000 cm^{-1}) globally to sums of exponentials. Rather than performing simultaneous exponential fits of the time courses at all 415 wavelengths, we reduced the complexity of the nonlinear fitting procedure by first obtaining a SVD of the data (15).

SVD provides a different way of representing our original two-dimensional data matrix (**A**, a set of absorbance changes measured at 415 wavelengths and 200 times). The new representation consists of three matrices (**U**, **S**, and **V**) that are defined by the properties that (*a*) $\mathbf{A} = \mathbf{USV}^T$, (*b*) **U** and **V** each consist of columns of orthonormal vectors, and (*c*) **S** is a diagonal matrix. The 415-element columns of **U** are called basis spectra, whereas the 200-element columns of **V** are designated time courses. The diagonal elements of **S** are termed the singular values of **A**, and the size of the *n*th singular value indicates the extent to which the *n*th columns of **U** and **V** contribute to **A**. The diagonal elements of **S** are arranged in

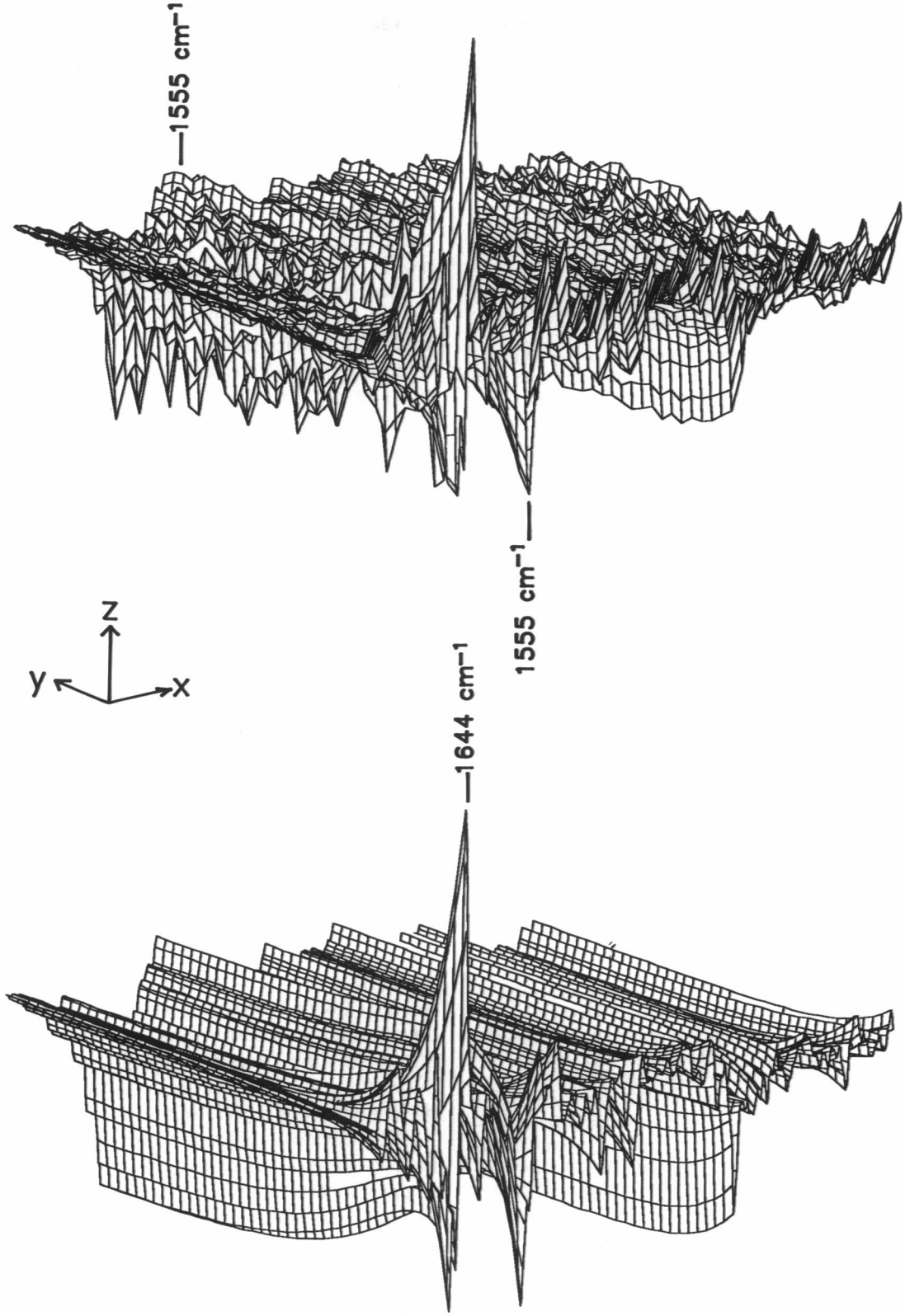

FIGURE 1 (*Top*) A time series of rhodopsin photoproduct difference spectra measured at pH 8 and 20°C. The wavenumber (*x*-axis) scale runs from 1,800 to 1,000 cm^{-1} (left-to-right) and the time (*y*-axis) scale from 0.25 to 100 min (front-to-back) after the illumination was turned off. To simplify the plot, only every fifth measured time slice is shown, corresponding to 2.5-min temporal spacing between the plotted data. The largest peak plotted, at 1,644 cm^{-1}, and the earliest time corresponds to an absorbance change of $+7.5 \times 10^{-3}$. (*Bottom*) A plot of the two-exponential decay process that gave the best least-squares fit to the measured data. The time constants and amplitudes at each wavelength were calculated by means of SVD, as described in the text.

order of decreasing singular value, and the columns of U and V are ordered correspondingly. The consequence of this arrangement is that the product of the first n columns of U, the $n \times n$ upper-left-hand corner of S, and the first n rows of $\mathbf{V}^T$ gives the best nth-order approximation to A (15).

Thus, the most significant basis spectra and time courses, i.e., those with the highest singular values, provide a close approximation to the measured absorbance changes at all wavelengths and times, whereas the information contained in the least significant basis spectra and time courses, i.e., those with lower singular values, are likely to contribute only noise at all wavelengths and times and can be discarded. For a multiexponential spectral decay process, one expects to obtain the same time constants by fitting the nonnoise time courses from the SVD as by fitting globally all wavelengths in the original spectral data set (15). As a consequence, SVD followed by matrix truncation makes it possible to include most of the measured signal and very little of the noise in a reduced data set useful for a simplified global exponential fit.

For each pH value, we found that three basis spectra from the SVD and their corresponding time courses were sufficient to represent the kinetic spectral data to within the level of the measured noise ($\sim 10^{-4} A$ at wavelengths outside the amide I region). These three most significant SVD components for the pH 8 data are shown in Fig. 2, along with the fourth most significant component for comparison. The basis spectra appear at left, scaled by their singular values; these spectra correspond to columns of the matrix US. The associated time courses (i.e., rows of $\mathbf{V}^T$) are plotted at right.

The time course associated with the fourth component (Fig. 2 *H*) shows a very fast exponential decay above the noise ($\tau \simeq 1$ min). This is probably due to decay of a small amount of meta I that is still present at this pH at the end of the illumination period. However, the singular value associated with this fourth component is still two orders of magnitude smaller than any of the largest three. In the case of the experiments at pH 5.5 and pH 7, the fourth component of the SVD was even smaller than at pH 8, and the associated time course was completely random in appearance (data not shown). Therefore, for all the pH values, only the first three spectral components and their associated time courses were used in subsequent calculations.

Kinetic fitting of spectra

The three time courses (rows of $\mathbf{V}^T$) obtained from each SVD were subjected to a global three-exponential fit. One of the rate constants was constrained to be 0; the other two were defined to be κ_1 and κ_2. Inclusion of an additional exponential did not significantly improve the fit. At each pH, optimum values of κ_1, κ_2, and all nine exponential coefficients were determined using a least-squares criterion. For the pH 8 example, the fitted curves appear in Fig. 2 superimposed on the SVD time courses. The weighted residual errors appear above the fitted curves.

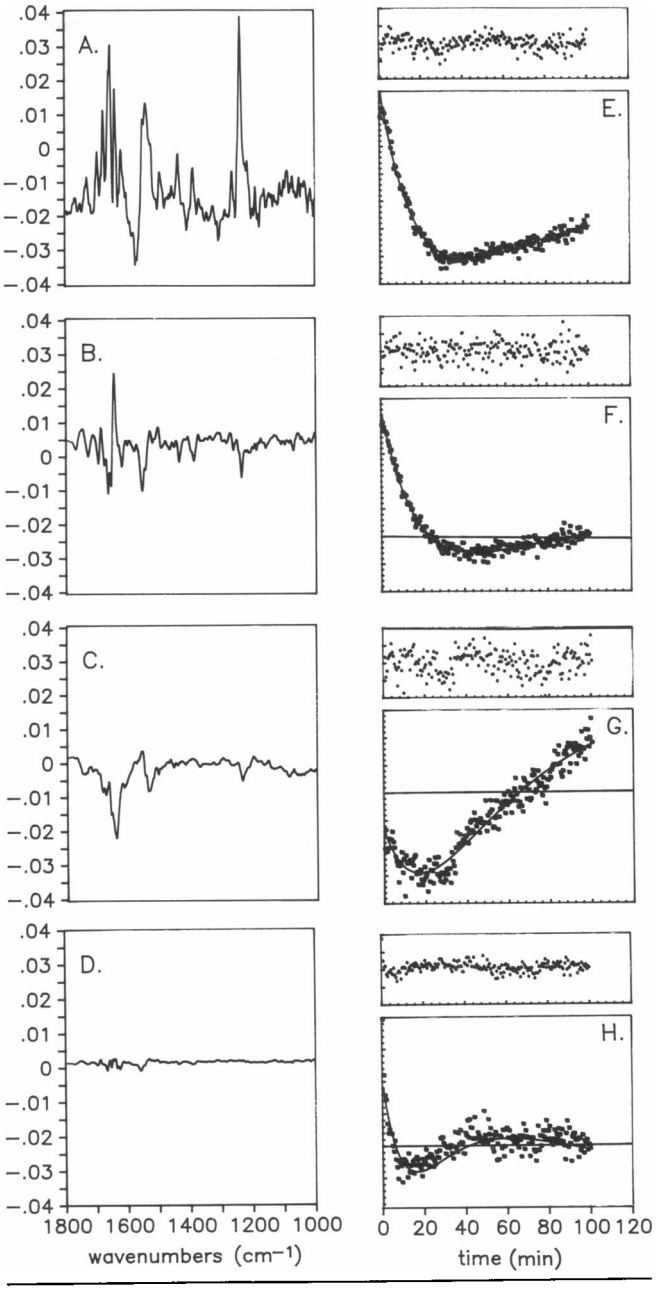

FIGURE 2 The first four components from the SVD of the data shown in Fig. 1. SVD reformulates the original data matrix of absorbance differences (A) as the product of three matrices: $\mathbf{A} = \mathbf{USV}^T$. (*A–D*). The first four columns of US, displayed as individual basis spectra. (*E–G*). The first three columns of V, displayed as time courses (or vector amplitudes). In each plot, a horizontal line extending the width of the box indicates the *y*-axis zero (in *E*, this horizontal line is coincident with the top of the box). The least-squares global exponential fit to the first three time courses is superimposed on the plotted data. The weighted residuals from this fit are shown above each time course. As shown in *H*, the fourth time course was also subsequently fit, but with two time constants constrained to values determined from the earlier fit, plus a third unconstrained time constant.

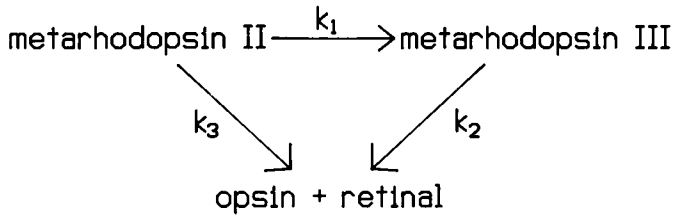

SCHEME 1

The nine exponential coefficients from the fit constitute the 3 × 3 **F**-matrix in the following expression, where $\mathbf{t} = (t_1, t_2, \ldots, t_{200})$:

$$\mathbf{A} = \mathbf{USV}^T \simeq \mathbf{U'FT} \simeq \mathbf{U'} \cdot \begin{bmatrix} F_{10} & F_{11} & F_{12} \\ F_{20} & F_{21} & F_{22} \\ F_{30} & F_{31} & F_{32} \end{bmatrix} \begin{bmatrix} \exp(-0\mathbf{t}) \\ \exp(-\kappa_1\mathbf{t}) \\ \exp(-\kappa_2\mathbf{t}) \end{bmatrix}. \quad (1)$$

As expected (15), the matrix product of **U'** (the first three columns of **US**) with **FT** (the exponentially fitted approximation to the first three rows of $\mathbf{V}^T$) gives a fairly accurate representation of the original spectral data with much of the noise filtered out, as shown in the bottom part of Fig. 1.

The apparent rate constants (κ_1 and κ_2) from the fits at all three pH values are given in Table 1. They are a factor of two to three slower than those obtained from visible spectroscopy at similar temperature and pH (3, 16). However, our value of $\kappa_1 = 4.5\ h^{-1}$ at pH 5.5 and 7 corresponds quite closely with the meta II spectral half-life of ~7 min observed in earlier FTIR work (8), which was performed at an unspecified pH. The discrepancy with the visible spectroscopic work may result from the lower amount of water or poorly controlled salt concentration present in FTIR samples. We were not able to increase the water content and still make the IR measurements with adequate signal-to-noise ratios.

Calculation of the difference spectra of the intermediates based on a kinetic model

The number of significant components in the SVD of the difference spectra (in this case three) is expected to be equal to the number of distinct photoproducts present during the experiment (15). The detection of only two apparent rate constants also limits the number of photointermediates to three, but does not limit the number of microscopic rate constants. A branched model with three microscopic rate constants (see Scheme 1) is the one most generally accepted based on visible absorption spectroscopy (17). In this model, meta II decays to opsin and retinal through two pathways: one via the intermediate meta III and the other via direct hydrolysis of the unprotonated Schiff base in meta II.

Equations describing the time-dependent concentrations of meta II, meta III, and opsin can be obtained by solving the differential equations that describe the model shown in Scheme 1. This model predicts that the time-dependent concentrations of all the intermediates can be expressed as sums of two exponentials and a constant. One of these exponentials has a rate constant equal to k_2, the microscopic rate constant for conversion of meta III into opsin. The other has a rate constant equal to $k_1 + k_3$; that is, to the sum of the rates of meta II decay to meta III and to opsin. As discussed above, this prediction of two apparent rate constants was borne out by our experimental results. Based on visible spectroscopy (18), $k_1 + k_3$ is expected to correspond to the faster of our two apparent constants (κ_1), whereas k_2 is expected to correspond to the slower (κ_2).

The difference spectrum at any time after bleaching should be describable as a linear combination of the "pure" difference spectra of the three photointermediates, with coefficients proportional to the relative photointermediate concentrations predicted by the kinetic model above. For our model (Scheme 1), the expected time dependence of the difference spectrum is given by the following matrix equation (which is derived in an analgous fashion to Eq. 2 of reference 12):

$$\mathbf{A} = (\Delta\mathbf{A}_{\text{rho}\rightarrow\text{meta II}} \quad \Delta\mathbf{A}_{\text{rho}\rightarrow\text{meta III}} \quad \Delta\mathbf{A}_{\text{rho}\rightarrow\text{opsin}}) \times \begin{bmatrix} 0 & 1 & 0 \\ 0 & -k_1/(k_1+k_3-k_2) & k_1/(k_1+k_3-k_2) \\ 1 & (k_2-k_3)/(k_1+k_3-k_2) & -k_1/(k_1+k_3-k_2) \end{bmatrix} \times \begin{bmatrix} \exp(-0\mathbf{t}) \\ \exp(-(k_1+k_3)\mathbf{t}) \\ \exp(-k_2\mathbf{t}) \end{bmatrix}. \quad (2)$$

Here the pure photointermediate difference spectra ($\Delta\mathbf{A}_{\text{rho}\rightarrow\text{meta II}}$, etc.) are expressed as column vectors, each with the same number of elements as the original columns of **A**.

The right-hand sides of Eqs. 1 and 2 can be equated, since they both describe the time evolution of the measured difference spectrum. Furthermore, the identification of κ_1 with $k_1 + k_3$ and κ_2 with k_2 means that the right-most matrices in both equations, which express all of the time dependence, are equal term by term. They can therefore be dropped from the equated expressions, leaving:

$$(\Delta\mathbf{A}_{\text{rho}\rightarrow\text{meta II}} \quad \Delta\mathbf{A}_{\text{rho}\rightarrow\text{meta III}} \quad \Delta\mathbf{A}_{\text{rho}\rightarrow\text{opsin}}) \times \begin{bmatrix} 0 & 1 & 0 \\ 0 & -k_1/(k_1+k_3-k_2) & k_1/(k_1+k_3-k_2) \\ 1 & k_2-k_3/(k_1+k_3-k_2) & -k_1/(k_1+k_3-k_2) \end{bmatrix} \simeq \mathbf{U'F}. \quad (3)$$

The photointermediate difference spectra, described by the leftmost matrix in Eq. 3, can be calculated by

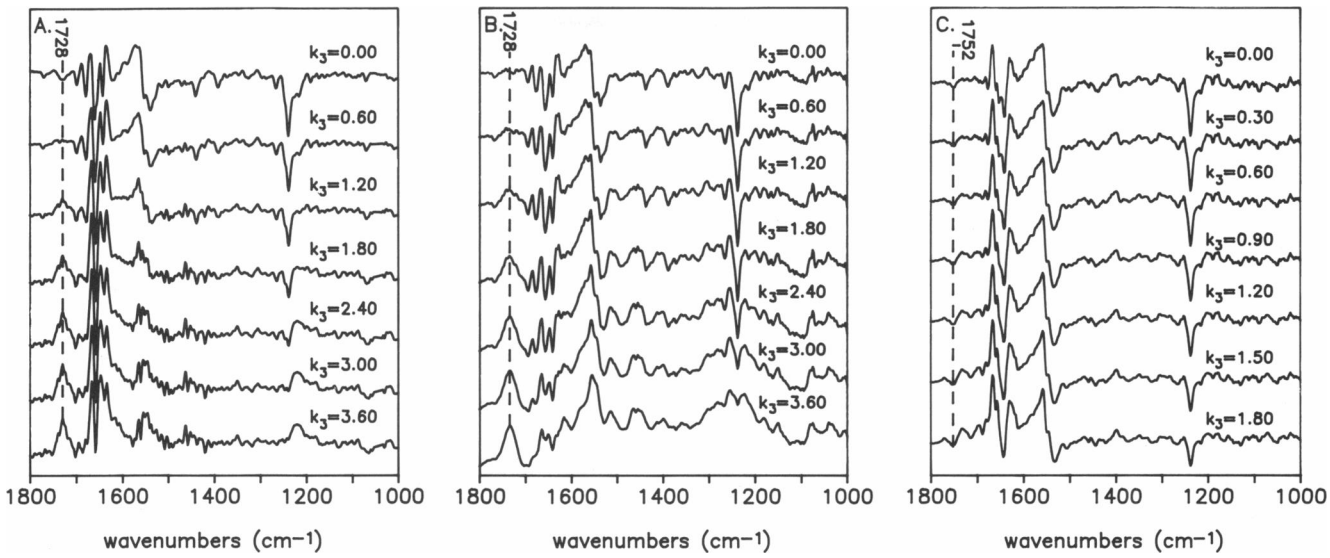

FIGURE 3 Three families of possible rho → meta III spectra for (*A*) pH 5.5, (*B*) pH 7, and (*C*) pH 8, calculated by assuming the indicated values for k_3 (h^{-1}), the microscopic rate constant for direct hydrolysis of meta II into opsin and retinal. The value for κ_1, the faster of the two apparent rate constants obtained from the exponential fit to the data (see Table 1), is the maximum possible value for k_3 and thus limits the range of values that need to be examined at each pH.

multiplying **U'F** on the right by the inverse of the rate constant matrix that appears in the equation. However, our model, in which there are more microscopic rate constants than apparent rate constants, permits an unambiguous calculation of only two of the three photointermediate difference spectra, since the individual values of k_1 and k_3 cannot be determined a priori from the apparent rate constants. A close examination of Eq. 3 will show that the elements in the inverted rate constant matrix that determine the rho → meta II and rho → opsin spectra turn out to be completely independent of k_1 and k_3. However, calculation of the rho → meta III spectrum requires assuming individual values for k_1 and k_3, subject to the empirical constraint $k_1 + k_3 = \kappa_1$.

Range of possible rho → meta III difference spectra

Fig. 3 shows a sampling from the families of possible rho → meta III difference spectra that are generated by assuming various values of k_3 (always setting $k_1 = \kappa_1 - k_3$). Over the full range of possible k_3 values, peak frequencies are relatively unchanged. However, the peak intensities are strongly dependent on k_3, in some cases changing sign between its extreme allowed values (see, for example, the 1,728-cm^{-1} band in Fig. 3, *A* and *B*).

Notably, these variations in peak intensity with choice of k_3 are greatly reduced for the pH 8 series (Fig. 3 *C*). All of these possible rho → meta III spectra are significantly different from previously published difference spectra of meta II decay products. For example, in the earlier work (8), a positive band persisted near 1,745 cm^{-1} in the photoproduct difference spectrum even at a time of 15 min after illumination. However, our results show no significant positive band near 1,745 cm^{-1} in any of the possible rho → meta III difference spectra in Fig. 3 *C*; only a negative band at 1,752 cm^{-1} appears in this region. The absence of a ~1,745-cm^{-1} positive band in the rho → meta III difference spectrum could not be ascertained from previously published data or even from our own data at lower pH (Fig. 3, *A* and *B*), which are ambiguous about the signs of rho → meta III difference bands in the 1,800–1,700-cm^{-1} spectral region. By obtaining time-resolved spectral data at high pH, we have placed significant new constraints on the spectrum of meta III and thus on its structure.

Not all of the possibilities in Fig. 3 are equally likely to represent the true rho → meta III difference spectrum. Some of the spectra at each pH are simply too unlike any of the spectra at other pH values to represent the same photointermediate protein conformation. For example, the pH 7 spectra with $k_3 \geq 2.4$ (Fig. 3 *B*) show an amide II difference bandshape (near 1,550 cm^{-1}) that is greatly dissimilar from any of the possible spectra at pH 8 (Fig. 3 *C*). Such observations suggest that the correct k_3 values are likely to be those that result in the least pH dependence of the calculated rho → meta III spectrum. Although our data show that this assumption can be correct only to a first approximation (see below for further details), it is nevertheless useful for objectively constraining k_3 to a more specific value at each pH. Accordingly, values of k_3 at the three different pH values were selected that minimized the grand sum of the squares of the differences between the three resulting calculated

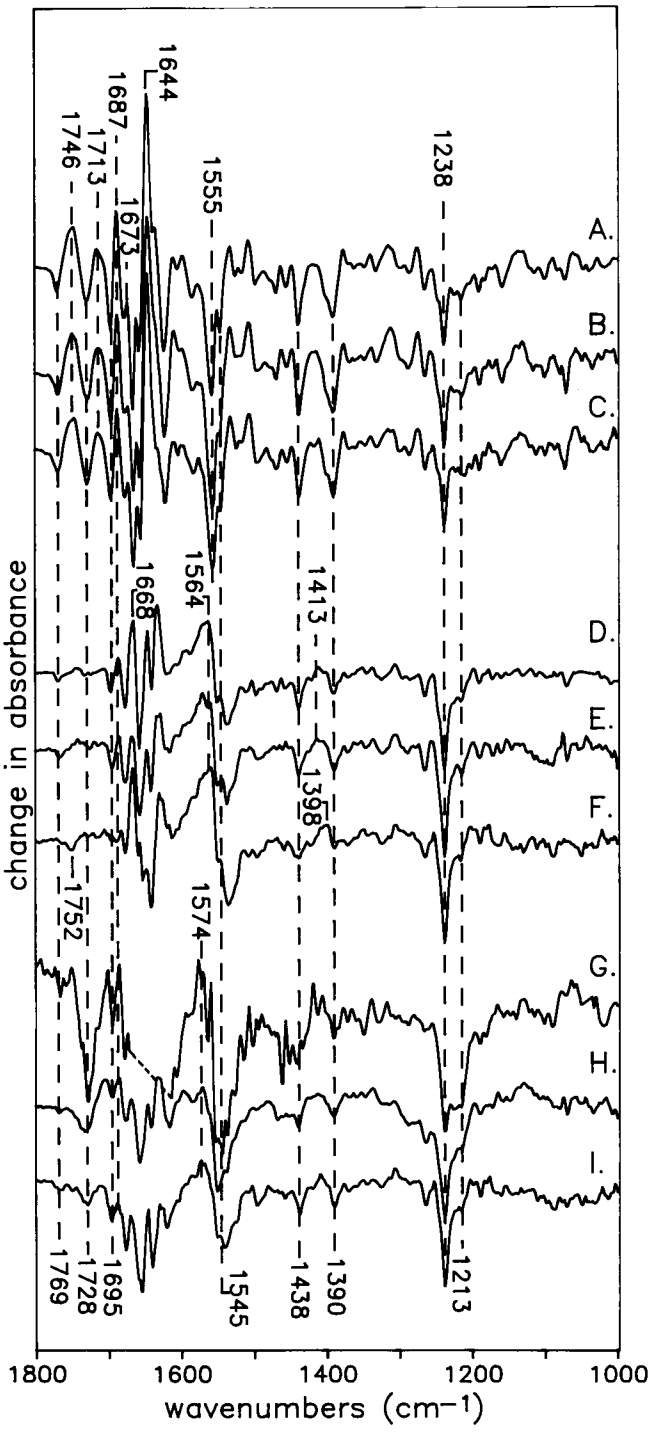

FIGURE 4 Calculated difference spectra for (*A–C*) rho → meta II, (*D–F*) rho → meta III, and (*G–I*) rho → opsin + retinal transitions at (*A,D,G*) pH 5.5, (*B,E,H*) pH 7, and (*C,F,I*) pH 8. Each set of three photointermediate difference spectra obtained at the same pH is plotted at a consistent vertical expansion (as determined by the kinetic analysis). The three sets obtained at different pH values were scaled to one another by eye, since the relative concentrations of the different samples in the IR cell were not measured precisely.

rho → meta III spectra. (The three rho → meta III difference spectra were always normalized before subtracting them from each other.) The resulting optimized rho → meta III spectra at pH 5.5, 7, and 8 are compared in Fig. 4, *D–F*, respectively. The optimal values of k_3 used to generate these spectra are presented in Table 1.

Fig. 4 also presents the rho → meta II and rho → opsin spectra at the same pH values. As stated above, calculation of these spectra required no assumptions about the values of the rate constants.

pH dependence of the photointermediate spectra

The rho → meta II difference spectrum is extremely insensitive to pH. Our calculated spectra at pH values ranging from 5.5 to 8 (Fig. 4, *A–C*) are all identical with rho → meta II difference spectra previously obtained at a number of other temperatures (8, 9, 14).

The rho → meta III difference spectra calculated at pH 5.5 and 7 (Fig. 4, *D* and *E*) are virtually superimposable outside of the region of strong background water absorbance (1,680–1,640 cm^{-1}), where spectral changes are likely to represent noise. However, the pH 8 spectrum (Fig. 4 *F*) differs significantly from the lower-pH spectra (Fig. 4, *D* and *E*) in at least three regards. (*a*) A negative peak shifts from 1,769 to 1,752 cm^{-1}. Both frequencies are appropriate for carbonyl stretching vibrations of protonated carboxylic acids. (*b*) A new positive peak appears at 1,398 cm^{-1}. This band is in the frequency region where the symmetric stretch vibration of a deprotonated carboxylate group would be expected. (*c*) A negative/positive difference feature that occurs at 1,695/1,687 cm^{-1} in the pH 5.5 and pH 7 spectra (Fig. 4, *D* and *E*) almost disappears at pH 8 (Fig. 4 *F*). Unlike some of the other features near the noisy amide I region, this feature's size is very reproducible in the two low pH experiments, so that its intensity decrease in the high-pH spectrum is significant.

The rho → opsin + retinal spectrum also is pH dependent but apparently has a lower pK_a than the rho → meta III spectrum. That is, among the set of rho → opsin difference spectra (Fig. 4, *G–I*), it is the one obtained at pH 5.5 that is dissimilar from the others, as evidenced most clearly by increased negative bands at 1,213 and 1,728 cm^{-1}. It is not surprising to see pH dependence of bands in the rho → opsin FTIR difference spectrum, because visible spectra of the "opsin + retinal" products have been shown to be pH dependent in solution studies (18, 19). We refer somewhat inaccurately to the final state of the protein as a mixture of opsin plus retinal. On hydrolysis of its linkage to Lys-296, 50% of the retinal goes on to form Schiff bases with other lysine residues of the protein, 30% forms Schiff bases with phosphatidylethanolamine, and the remaining retinal remains free (7). It is quite reasonable that the nonspecific retinylidene Schiff bases might interact in a pH-dependent manner with external carboxylate groups of the protein (or of membrane phosphatidylserines).

TABLE 1 **Observed pH dependence of meta II decay components**

pH	Apparent rate constants*		Microscopic rate constants‡		
	κ_1	κ_2	k_1	k_2	k_3
	h^{-1}	h^{-1}	h^{-1}	h^{-1}	h^{-1}
5.5	4.50 ± 0.23	0.10 ± 0.01	4.13 ± 0.21	0.10 ± 0.01	0.37 ± 0.02
7.0	4.48 ± 0.12	0.46 ± 0.04	4.22 ± 0.11	0.46 ± 0.04	0.26 ± 0.01
8.0	2.82 ± 0.06	1.80 ± 0.08	2.81 ± 0.06	1.80 ± 0.08	0.00 ± 0.01

* These parameters gave the best least-squares fit to the matrix equation $\mathbf{V}(t) = (1 \exp - \kappa_1 t \exp - \kappa_2 t) \cdot \mathbf{F}$, where $\mathbf{V}(t)$ represents the first three time courses from the SVD (shown in Fig. 2 for the pH 8 data only). The nine values for the F matrix were also optimized for each pH value (results not shown).

‡ These values are for the model shown in Scheme 1. As described in the text, k_1 and k_3 were obtained by a computer search, subject to the constraint $k_1 + k_3 = \kappa_1$, for the values that minimized the variance between the resulting normalized rho → meta III spectra at the three pH values.

pH dependence of the microscopic rate constants

Our approach yields values for k_3, the rate of direct conversion of meta II to opsin, which decrease monotonically with increasing pH (Table 1). This pH dependence is qualitatively similar to that observed previously. In particular, solution studies have shown that the percentage of meta II hydrolyzed directly into opsin decreases at high pH (18). Conversely, our data are consistent with an increase in k_2 at high pH. The pH dependence of this, the rate constant for decay of meta III to opsin, apparently has not been examined previously.

Our results do not show the increase in rate of formation of meta III (k_1) with increasing pH that was seen in both solution and suspension studies (18, 20). On the contrary, we see a approximate twofold decrease in k_1 at the highest pH value (Table 1). One possible explanation for this discrepancy is that our assumption of pH independence for the rho → meta III difference spectrum is in error. However, this explanation is probably inadequate. The only way our data could be made consistent with an increase in k_1 between pH 5.5 and 8 would be if the value of k_1 at pH 5.5 were $>1.3\ h^{-1}$ less than the value of $4.13\ h^{-1}$ (Table 1) that was derived by using our assumption. In this case, the constraint $k_1 + k_3 = \kappa_1$ would result in a high value ($>1.3\ h^{-1}$) for k_3, which would in turn limit the rho → meta III difference spectrum at pH 5.5 to a range of possibilities (see bottom four spectra of Fig. 3 *A*) that are all very different from any of the possible spectra at pH 8 (Fig. 3 *C*). Instead, our observation of a decrease in k_1 at high pH, where others see an increase, is likely to be due to the different sample conditions used for IR and visible spectroscopy (especially the sample's ionic strength).

DISCUSSION

Assumptions involved in calculating the rho → meta III difference spectra

With anything other than an unbranched irreversible reaction pathway, one generally expects a degenerate set of solutions for a calculation of photointermediate difference spectra from observed time-resolved absorbance changes. As has been discussed at some length in the case of visible absorption spectra (21), one way to break this degeneracy is to assume that the photointermediate spectra should not exhibit any strong temperature dependence. Our approach in constraining the rho → meta III spectrum, which involves an assumption of approximate pH independence, is somewhat analogous. Both temperature and pH changes permit breaking the degeneracy in the spectral calculations by shifting the relative branching between two distinct pathways.

Although it might seem that pH would be more likely to affect a vibrational spectrum of a protein with many titratable groups than would a temperature change, we chose pH initially because of some important experimental details. First, to obtain the best signal-to-noise ratio in the derived spectra, it was important that the branching ratio for the two decay paths be changed significantly by the change in conditions. This would have required examining a significant temperature range, probably covering ≥15°C. Cooling the sample this far below ambient temperature would have increased the lifetime of meta III beyond the ~4-h period over which our instrumental baseline was stable and would also have caused increased contributions from a fourth photoproduct (meta I). On the other hand, warming above room temperature would have raised concerns about stability of the sample, which must be maintained at the measurement temperature for several hours before the spectral baseline becomes sufficiently invariant even to begin a 2-h FTIR difference measurement.

Since we are dealing only with difference spectra, our assumption of pH independence is not as problematic as it might first appear. For the most part, amino acid side chains with a pK_a within our experimental range (at least those that are remote from the active site) will have the same protonation state in both rhodopsin and meta III. Such residues are therefore not expected to contribute to the rho → meta III difference spectrum. Of course, it is possible that there are titratable groups whose pK_a

values are different in rhodopsin and meta III, for example, groups that are solvent accessible in meta III but not in rhodopsin. In this case, one would certainly expect differences in the rho → meta III spectra measured at different pH values. As we have shown, however (see Results), such protonation changes are likely to be rather localized and not to give rise to additional protein rearrangements comparable in size to those that occur between different photointermediate states. Such large rearrangements should cause a significant shift in λ_{max}, whereas no visible spectral shifts of the meta III intermediate have been identified in pH studies of the decay of meta II (18).

For such reasons, all photointermediates with well-defined pH-independent visible spectra are also expected to exhibit FTIR difference spectra that are largely pH independent, especially in the amide I and amide II spectral regions indicative of peptide backbone conformation. It should be noted again that the rho → meta II and rho → opsin(+retinal) difference spectra in Fig. 4 were calculated without assuming they were pH independent. The fact that they nevertheless turn out to show very little pH dependence, especially rho → meta II, is a useful confirmation of the reasonableness of our approach.

At the same time, further analysis demonstrates that the assumption of pH independence for the rho → meta III spectrum can be accurate only to a first approximation. There were several small difference bands in this photointermediate's spectrum that change with pH, regardless of the k_3 values assumed. However, this did not seem to interfere with our overall approach for determining the value for k_3 and the rho → meta III spectrum at each pH. Evidently, the large spectral features near 1,550 cm^{-1} (Fig. 3), which are probably characteristic of a peptide backbone conformation involving several residues (see below), are more heavily weighted than any individual side chain bands in the search for the best values of k_3. As a result, the latter pH-dependent bands do not prevent convergence of other frequency regions to well defined consensus bandshapes nor are the pH-dependent bands completely suppressed in the optimized spectra.

Structural comparisons between meta II and its decay products

It is noteworthy that, despite the minor pH dependence of both the rho → meta III and rho → opsin + retinal difference spectra, the strongest features in both are generally pH independent and characteristically different from features seen in the rho → meta II spectrum. Most notably, the positive 1,746- and 1,713-cm^{-1} bands in the rho → meta II spectrum (Fig. 4, *A–C*) are absent in spectra of both later photoproducts, as are the large positive band in the amide I region at 1,644 cm^{-1} and negative band in the amide II region at 1,555 cm^{-1}. In place of these characteristic rho → meta II features, the rho → meta III (Fig. 4, *D–F*) and rho → opsin (Fig. 4, *G–I*) difference spectra exhibit a general absence of large difference bands, other than (*a*) a rather broad amide II difference feature with a positive peak at ~1,565 cm^{-1} and a negative peak at ~1,535 cm^{-1} and (*b*) a negative 1,238-cm^{-1} band that is probably due to the retinal chromophore of rho (22). Below we discuss in detail some possible structural implications for the spectral differences between meta II and its thermal decay products.

Carboxylate residue side chain protonation states

One of the hallmarks of the rho → meta II difference spectrum (Fig. 4, *A–C*) is the pattern of positive and negative bands between 1,700 and 1,800 cm^{-1}. This IR spectral region is the simplest to interpret, because there are a limited number of possible assignments for these bands. In ROS preparations, the only strong characteristic group vibrations in this frequency range are C=O stretches of lipid esters and protonated carboxylic acid side chains of aspartic or glutamic acid. All of the absorbance difference peaks in the 1,700–1,800-cm^{-1} region of the rho → meta II difference spectrum have been assigned previously to the latter, based on their insensitivity to substitution of native ROS lipids with ether-linked phosphatidylcholine (23).

Our data (Fig. 4) show that the carboxylic acid structural changes involved in meta II formation still occur at pH 8.0, i.e., far above the pK_a value of Asp or Glu side chains in aqueous solution. Thus, even though most of these peaks have been shown to be sensitive to ^2H_2O exchange (23), the Asp or Glu side chains giving rise to them must have pK_a values above 8 and must therefore be buried in nonpolar environments in both rho and meta II.

By the time meta III is formed, the large difference bands in the COOH region have essentially disappeared (Fig. 4, *D–F*). As has been discussed previously (8), this indicates that the COOH-group reactions giving rise to these bands are reversed during decay of meta II. However, earlier work left it unclear whether this structural reversal was complete on formation of meta III or required further decay to opsin. Our results indicate that the former is true. In fact, our data indicate that new COOH-group perturbations occur when meta III decays to opsin, as evidenced by the large negative peak at 1,728 cm^{-1} in Fig. 4, *G–I*.

The clear association of meta II → meta III decay with loss of transducin-activation capabilities (3) suggests that the Asp or Glu residues giving rise to the 1,713, 1,728, 1,746 and 1,769 cm^{-1} bands in the rho → meta II difference spectrum are specifically involved in transducin binding or activation. Recently, Ganter et al. (14) proposed that these peaks indicate the protonation of one Glu or Asp residue (1,713 cm^{-1}), deprotonation of a second Glu or Asp (1,728 cm^{-1}), and a change in hydro-

gen bonding of third (1,746 and 1,769 cm^{-1}). The frequencies of the latter two peaks indicate that this third residue is protonated in both rho and meta II. Assignment of both peaks to a single residue was based partially on the presence of the 1,769-cm^{-1} negative band in difference spectra of earlier intermediates, along with positive peaks at somewhat different frequencies than the 1,746-cm^{-1} frequency observed in the rho → meta II difference spectrum. This would suggest that the hydrogen bonding environment of the same COOH group is being modulated in all of the rhodopsin photointermediates.

However, our difference spectra do not support the idea that this same COOH group continues to be modulated in the meta III state. Whereas the negative 1,769-cm^{-1} band in the rho → meta II difference spectrum is pH invariant (Fig. 4, *A–C*), the very small negative 1,769-cm^{-1} band in the rho → meta III difference spectrum at lower pH values (Fig. 4, *D* and *E*) appears to shift to 1,752 cm^{-1} at pH 8 (Fig. 4 *F*). Thus, in addition to the three Asp or Glu residues detected by Ganter et al. [14), there appears to be a fourth, which at low pH also has a COOH frequency of ~1,769 cm^{-1}. However, its frequency appears to downshift by 17 cm^{-1} at pH 8. Other changes in the pH 8 rho → meta III spectrum (Fig. 4 *F*) that appear to be correlated with the downshift of the 1,769-cm^{-1} COOH vibration are as follows: (*a*) a small positive band in the COOH region (1,740 cm^{-1}) is eliminated, whereas (*b*) a new positive band in the COO^- symmetric stretch region (1,398 cm^{-1}) appears. One possible interpretation of these changes is that meta III formation at pH 8 involves deprotonation of a carboxylic acid, whereas this same COOH group merely undergoes hydrogen bond alteration during meta III formation at pH 7 and below. These pH-dependent effects could be explained most easily if this COOH group were near to a titratable histidine residue (e.g., His211). At lower pH values, the presence of the positively charged histidine could explain the lowering of the vibrational frequency of the nearby COOH group in the rho state, as well as the lowering of its pK_a in meta III.

To summarize, our results suggest that the three COOH groups hypothesized to give rise to the 1,769-, 1,746-, 1,728-, and 1,713-cm^{-1} bands experience a large structural perturbation only in the meta II state. This might be expected if all of these carboxylic acid groups are uniquely affected by a cooperative structural change required for the binding and activation of transducin.

Other amino acid side chains

There is a positive band at 1,673 cm^{-1} in the rho → meta II difference spectra at all pH values (Fig. 4, *A–C*) that is absent, or possibly downshifted to 1,668 cm^{-1}, in the spectra of the later intermediates (Fig. 4, *D–I*). The 1,673-cm^{-1} band is at exactly the right frequency for the antisymmetric C=N stretch of an arginine residue (24). However, it also lies within the frequency range for the amide I (C=O stretch) vibration of a peptide group (see below) or an asparagine or glutamine side chain. The previously observed disappearance of this band on ^2H_2O exchange, concomitant with an intensity increase at 1,610 cm^{-1} (14), tends to support the arginine assignment, since the latter frequency is where deuterated arginine side chains are expected to absorb (25).

The positive 1,673-cm^{-1} meta II difference peak (Fig. 4, *A–C*) could thus signal the presence of an arginine structural change between rho and meta II, which is reversed when meta III or opsin is formed (Fig. 4, *D–I*). This is an intriguing hypothesis, since it has been shown by site-directed mutagenesis of rhodopsin that arginine-135 (which is highly conserved in G-protein-coupled membrane receptors) is probably involved in transducin activation (26, 27).

Chromophore vibrations

A negative band at 1,238 cm^{-1} that is present in the rho → meta II difference spectrum becomes larger in the difference spectra of both later intermediates. Since it is negative, it must correspond to a rho vibration. The only way that this negative intensity can increase during meta II decay is if there is a positive band in the meta II spectrum that partially cancels the 1,238-cm^{-1} negative intensity, and the structure giving rise to this positive band is eliminated when meta II decays. This structure is probably the unprotonated Schiff base chromophore of meta II, which has a resonance Raman vibrational band at 1,231 cm^{-1} (28). Presumably this positive meta II IR band shifts to a different frequency when the chromophore is reprotonated (to form meta III) or hydrolyzed (to form opsin), resulting in a larger negative 1,238-cm^{-1} band in the difference spectra of these later photoproducts.

Another feature that is probably due to the chromophore is the negative band observed as a shoulder at ~1,545 cm^{-1} in all of the spectra in Fig. 4. This band is due to the rho state and coincides with the chromophore ethylenic stretching vibration observed in the resonance Raman spectrum of rho (22). Likewise, the negative 1,390-cm^{-1} band present in all of the photointermediate difference spectra of Fig. 4 coincides with a resonance Raman band of rhodopsin and is thus likely to be due to the rho chromophore.

Peptide backbone conformation

The amide I (1,690–1,620 cm^{-1}) and amide II (1520–1565 cm^{-1}) vibrations of the peptide group are well known to be sensitive to secondary structure (29). Our results clearly confirm earlier work (8), indicating that that meta II has a protein backbone conformation that is unique among the late visual pigment photoproducts. This unique conformation is evidenced by rather large features at 1,644 (positive) and 1,555 cm^{-1} (negative) in the amide I and amide II regions of its difference spec-

trum. Both of these features disappear on decay of meta II to either meta III or opsin and are furthermore invariant in the rho → meta II spectra obtained over a significant pH range (Fig. 4, *A–C*). The 1,644-cm^{-1} band is in a frequency region appropriate for α-helical structure (29). As discussed previously (8), the size of this band is consistent with just a few peptide bonds undergoing a secondary structural rearrangement during formation of meta II. Another amide I feature in the rho → meta II spectrum that gets smaller in both rho → meta III and rho → opsin difference spectra is the negative/positive difference band at 1,695/1,687 cm^{-1}. This feature is in an appropriate frequency range for the amide I vibration of a β-sheet or -turn structure (29); it is thus not likely to be due to the same peptide bond(s) giving rise to the 1,644-cm^{-1} difference band.

It thus appears that several different types of peptide bond conformations may be changing in a coupled fashion during the rho → meta II transition. Taken along with information given above, the amide I and amide II vibrational difference bands in the rho → meta II difference spectrum indicate that the key structural transformation of rho leading to transient formation of rho* is a protein backbone conformational rearrangement involving at most a few residues, that is tightly correlated with protonation or hydrogen bonding changes of three to four buried carboxylate groups, and possibly also with perturbation of an arginine side chain.

The similar appearances of the amide II (1,560–1,530 cm^{-1}) spectral regions in the rho → meta III and rho → opsin difference spectra (Fig. 4, *D–I*) suggest that meta III and opsin probably share nearly the same polypeptide backbone conformation. However, these amide II difference bands contrast strongly with those seen in the rho → meta II spectrum (Fig. 4, *A–C*), indicating that the meta III/opsin backbone structure is significantly different from that of meta II. It is important to recognize, however, that the meta III/opsin backbone structure also appears to be significantly different from that of the starting state (rho), as suggested by the large size of the amide II difference peaks in Fig. 4, *D–I*. These bands are nearly as intense as any seen in the amide I or amide II regions of the rho → meta II difference spectrum (Fig. 4, *A–C*). Thus, the refolding of the protein during meta II decay does not completely restore the original polypeptide backbone structure of rho but instead leaves the protein in a third distinct conformational state.

The apparent similarity of the peptide backbone structures in meta III and opsin indicates that these structures do not simply result from loss of the retinal chromophore from its binding pocket–unless, however, the protonated Schiff base attachment site in meta III is not at the same location as in rho (lysine-296). The reversibility of the meta I → meta II → meta III decay processes (3) argues against such a possibility; however, the site of chromophore attachment in meta III has never been proven directly.

We are grateful to Michael Johnson for help in using his multiexponential fitting program, and to Burton J. Litman, Drake Mitchell, and Julie Kibelbeck for assistance with sample preparations as well as for many useful discussions.

A. L. Klinger was supported by the National Institutes of Health Training Program in Molecular Biophysics (T32GM-08323). M. S. Braiman is a Lucille P. Markey Scholar, and this work was supported by a grant from the Lucille P. Markey Charitable Trust.

Received for publication 2 April 1992 and in final form 16 July 1992.

REFERENCES

1. Yoshizawa, T., and G. Wald. 1963. Pre-lumirhodopsin and the bleaching of visual pigments. *Nature (Lond.)*. 197:1279–1286.
2. Emeis, D., H. Kühn, J. Reichert, and K. P. Hoffmann. 1982. Complex formation between metarhodopsin II and GTP-binding protein in bovine photoreceptor membranes leads to a shift of the photoproduct equilibrium. *FEBS (Fed. Eur. Biochem. Soc.) Lett.* 143:29–34.
3. Kibelbek, J., D. C. Mitchell, J. M. Beach, and B. J. Litman. 1991. Functional equivalence of metarhodopsin II and the G_t-activating form of photolyzed bovine rhodopsin. *Biochemistry.* 30:6761–6768.
4. Stryer, L. 1986. Cyclic GMP cascade of vision. *Annu. Rev. Neurosci.* 9:87–119.
5. Matthews, R. G., R. Hubbard, P. K. Brown, and G. Wald. 1963. Tautomeric forms of metarhodopsin. *J. Gen. Physiol.* 47:215–240.
6. Ostroy, S. E., F. Erhardt, and E. W. Abrahamson. 1966. Protein configuration changes in the photolysis of rhodopsin. II. The sequence of intermediates in thermal decay of cattle metarhodopsin in vitro. *Biochim. Biophys. Acta.* 112:265–277.
7. Van Breugel, P. J. G. M., P. H. M. Bovee-Geurts, S. L. Bonting, and F. J. M. Daemen. 1979. Biochemical aspects of the visual process. XL. Spectral and chemical analysis of metarhodopsin III in photoreceptor membrane suspensions. *Biochim. Biophys. Acta.* 557:188–198.
8. Rothschild, K. J., J. Gillespie, and W. J. DeGrip. 1987. Evidence for rhodopsin refolding during the decay of Meta II. *Biophys. J.* 51:345–350.
9. Rothschild, K. J., W. A. Cantore, and H. Marrero. 1983. Fourier transform infrared difference spectra of intermediates in rhodopsin bleaching. *Science (Wash. DC).* 219:1333–1335.
10. Miller, J. L., D. A. Fox, and B. J. Litman. 1986. Amplification of phosphodiesterase is greatly reduced by rhodopsin phosphorylation. *Biochemistry.* 25:4983–4988.
11. Braiman, M. S., P. L. Ahl, and K. J. Rothschild. 1987. Millisecond Fourier-transform infrared difference spectra of bacteriorhodopsin's M_{412} photoproduct. *Proc. Natl. Acad. Sci. USA.* 84:5221–5225.
12. Chen, W.-G., and M. S. Braiman. 1991. Kinetic analysis of time-resolved infrared difference spectra of the L and M intermediates of bacteriorhodopsin. *Photochem. Photobiol.* 54: 905–910.
13. Johnson, M. L., and S. G. Frasier. 1985. Nonlinear least-squares analysis. *Methods Enzymol.* 117:301–342.
14. Ganter, U. M., E. D. Schmid, D. Perez-Sala, R. R. Rando, and F.

Siebert. 1989. Removal of the 9-methyl group of retinal inhibits signal transduction in the visual process. A Fourier transform infrared and biochemical investigation. *Biochemistry.* 28:5954–5962.

15. Henry, E. R., and J. Hofrichter. 1992. Singular value decomposition: application to the analysis of experimental data. *Methods Enzymol.* 210:129–192.
16. Watanabe, M., and H. Asai. 1980. Proton release and formation of photointermediates after light-induced proton uptake in bovine photoreceptor disc membranes. *Biochem. Biophys. Res. Commun.* 94:529–534.
17. Blazynski, C., and S. E. Ostroy. 1981. Dual pathways in the photolysis of rhodopsin: studies using a direct chemical method. *Vision Res.* 21:833–841.
18. Blazynski, C., and S. E. Ostroy. 1984. Pathways in the hydrolysis of vertebrate rhodopsin. *Vision Res.* 24:459–470.
19. Ostroy, S. E. 1974. Hydrogen ion changes of rhodopsin. *Arch. Biochem. Biophys.* 164:275–284.
20. Bennett, N. 1980. The decay of metarhodopsin II in cattle rod outer segment membranes: protonation and spectral changes. *Biochem. Biophys. Res. Commun.* 96:1695–1701.
21. Nagle, J. F. 1991. Solving complex photocycle kinetics. Theory and direct method. *Biophys. J.* 59:476–487.
22. Mathies, R., A. R. Oseroff, and L. Stryer. 1976. Rapid-flow resonance Raman spectroscopy of photolabile molecules: rhodopsin and isorhodopsin. *Proc. Natl. Acad. Sci. USA.* 73:1–5.
23. DeGrip, W. J., J. Gillespie, and K. J. Rothschild. 1985. Carboxyl group involvement in the meta I and meta II stages in rhodopsin bleaching. A Fourier transform infrared spectroscopic study. *Biochim. Biophys. Acta.* 809:97–106.
24. Venyaminov, S. Y., and N. N. Kalnin. 1990. Quantitative IR spectrophotometry of peptide compounds in water (H_2O) solutions. I. Spectral parameters of amino acid residue absorption bands. *Biopolymers.* 30:1243–1257.
25. Chirgadze, Y. N., O. V. Fedorov, and N. P. Trushina. 1975. Estimation of amino acid residue side-chain absorption in the infrared spectra of protein solutions in heavy water. *Biopolymers.* 14:679–694.
26. Franke, R. R., B. König, T. P. Sakmar, H. G. Khorana, and K. P. Hofmann. 1990. Rhodopsin mutants that bind but fail to activate transducin. *Science (Wash. DC).* 250:123–125.
27. Sakmar, T. P., R. R. Franke, and H. G. Khorana. 1989. Glutamic acid-113 serves as the retinylidene Schiff base counterion in bovine rhodopsin. *Proc. Natl. Acad. Sci. USA.* 86:8309–8313.
28. Doukas, A. G., B. Aton, R. H. Callender, and T. G. Ebrey. 1978. Resonance Raman studies of bovine metarhodopsin I and metarhodopsin II. *Biochemistry.* 17:2430–2435.
29. Venyaminov, S. Y., and N. N. Kalnin. 1990. Quantitative IR spectrophotometry of peptide compounds in water (H_2O) solutions. II. Amide absorption bands of polypeptides and fibrous proteins in α-, β-, and random coil conformations. *Biopolymers.* 30:1259–1271.